Large-Area Synthesis of Continuous and Uniform MoS_2 Monolayer Films on Graphene

Kathleen M. McCreary, Aubrey T. Hanbicki, Jeremy T. Robinson, Enrique Cobas, James C. Culbertson, Adam L. Friedman, Glenn G. Jernigan, and Berend T. Jonker**

Heterostructures composed of multiple layers of different atomically thin materials are of interest due to their unique properties and potential for new device functionality. MoS_2-graphene heterostructures have shown promise as photodetectors and vertical tunnel transistors. However, progress is limited by the typically micrometer-scale devices and by the multiple alignments required for fabrication when utilizing mechanically exfoliated material. Here, the synthesis of large-area, continuous, and uniform MoS_2 monolayers directly on graphene by chemical vapor deposition is reported, resulting in heterostructure samples on the centimeter scale with the possibility for even larger lateral dimensions. Atomic force microscopy, photoluminescence, X-ray photoelectron, and Raman spectroscopies demonstrate uniform single-layer growth of stoichiometric MoS_2. The ability to reproducibly generate large-area heterostructures is highly advantageous for both fundamental investigations and technological applications.

1. Introduction

Graphene has received much attention due to its intrinsic two-dimensional (2D) nature, high electronic mobility, linear band dispersion and exceptional crystalline quality.[1] In addition to fundamental scientific interest, it also promises to have significant technological impact on a variety of applications, including flexible electronics,[2] hydrogen storage,[3] gas sensing,[4,5] use as a conductive back plane,[6] and protective coatings.[7]

This diverse activity has stimulated interest into other 2D materials such as the transition metal dichalcogenides (e.g., MoS_2, $MoSe_2$, WS_2, and WSe_2).[8,9] These materials share the van der Waals-bonded layered structure of graphite, enabling isolation of single to few monolayer samples for analysis by mechanical[10] or chemical exfoliation.[11] Monolayer samples thus prepared exhibit properties that are strikingly different from the bulk and complement those of graphene, providing a suite of 2D materials suitable for a much broader range of applications. For instance, although bulk MoS_2 is an indirect gap semiconductor ($E_g \approx 1.3$ eV), in monolayer format it abruptly transitions to a direct gap semiconductor with strong excitonic luminescence at ≈1.8 eV.[12,13] Monolayer MoS_2 exhibits high optical responsivity and a quantum yield of 4×10^{-3},[12] in direct contrast to graphene, which displays inefficient light emission and quantum efficiency below 10^{-12}.[14] Transistors fabricated from MoS_2 monolayers demonstrate room temperature current on/off ratios in excess of 1×10^8 and ultralow standby power dissipation,[15] as well as highly selective chemical vapor sensors.[16] These properties suggest MoS_2 may be a promising material for integration into CMOS electronics and a valuable complement to graphene.[17–20] By combining graphene with MoS_2 it may be possible to utilize beneficial properties of each material.

A logical progression from the study of individual 2D materials leads to the combination of multiple films to form heterostructures. Very recently, heterostructure devices were successfully fabricated and characterized,[21–24] exhibiting unique and interesting properties. The MoS_2-graphene combination holds promise for use as a photodetector, as high photocurrents and persistent photoconductivity were demonstrated.[23] MoS_2 can also serve as a tunnel barrier for current injection into graphene in a field effect tunneling transistors,[22] a difficult task to accomplish on graphene due to its high surface diffusion and low chemical reactivity.

Typical heterostructure devices are produced via mechanical exfoliation and multiple stackings of the various 2D components,[22–24] limiting fabrication to a few micrometer-scale devices. Direct large-area growth of the desired 2D heterostructure is critical to enable large-scale device fabrication for technological applications. Chemical vapor deposition (CVD) is a successful means to produce large-area graphene,[2,25,26] with current technologies growing continuous films hundreds of meters in length using a roll-to-roll process.[27] Additionally, continuous films of MoS_2 were recently grown on insulating substrates.[28–30] While the synthesis of individual 2D materials was successfully demonstrated, the growth of heterostructures composed of multiple atomically thin 2D materials remains a key goal and challenge. Several recent reports provided important contributions to the nascent field of 2D heterostructure

Dr. K. M. McCreary, Dr. A. T. Hanbicki,
Dr. J. T. Robinson, Dr. E. Cobas, Dr. J. C. Culbertson,
Dr. A. L. Friedman, Dr. G. G. Jernigan,
Dr. B. T. Jonker
Naval Research Laboratory
Washington, DC 20375, USA
E-mail: kathleen.mccreary.ctr@nrl.navy.mil;
berry.jonker@nrl.navy.mil

DOI: 10.1002/adfm.201401511

synthesis. Nano-scale flakes of MoS_2 on graphene were achieved[31,32] as well as continuous MoS_2 films of varying thickness on epitaxial graphene,[33] and seeding promoted monolayer MoS_2 on mechanically exfoliated graphene.[34] Although progress is rapid, difficulties remain in the synthesis of large-area heterostructures with uniformity and thickness control.

2. Results and Discussion

In this paper, we report the growth by CVD of continuous and uniform MoS_2 single layer films on large-area graphene. The heterostructure films are characterized via atomic force microscopy (AFM), Raman spectroscopy, X-ray photoelectron spectroscopy (XPS), and photoluminescence (PL) spectroscopy. Direct large-area production of van der Waals heterostructures will make fundamental investigations of these systems more accessible to the scientific community, and is an important step towards incorporation of such devices into future technology.

A two-step CVD process is implemented to obtain heterostructure samples consisting of MoS_2 on graphene, with a supporting substrate of SiO_2/Si(001). In the first step, large-area, high quality graphene is grown by CVD on copper foil and transferred onto an SiO_2(275nm)/Si wafer following the procedure of Li et al.[25] The samples are annealed in forming gas to clean the graphene surface and improve adhesion. The graphene/SiO_2/Si is then introduced to a second tube furnace for the CVD growth of MoS_2. Solid sources of $MoCl_5$ and sulfur are used as precursors for the MoS_2 growth.[28] Both the substrate and $MoCl_5$ precursor are placed on a quartz platform at the center of a 2" diameter tube furnace, with a separation of 4–8 cm between $MoCl_5$ precursor and substrate, as shown in the schematic of **Figure 1**a. To achieve monolayer films of MoS_2 on graphene, 20 mg of $MoCl_5$ is used, with 1200 mg sulfur positioned at the upstream end of the furnace. Thicker films can be controllably synthesized by increasing the amount of $MoCl_5$. Two (three) layers are achieved using 35 mg (50 mg) of precursor. As the temperature is increased, the pressure is maintained at 2 Torr under a 50 sccm flow of Argon. Upon reaching 850 °C, the growth temperature is maintained for 10 min, and the sample is then allowed to cool undisturbed under continuous Ar flow.

Figure 1b shows an optical image of the resulting growth on graphene. The edge of the underlying graphene is identified via an arrow as a guide to the eye. The MoS_2 uniformly covers the graphene film and exposed SiO_2 areas, as evident in the optical image. The MoS_2-graphene film covers the area to the right of the arrow, while the MoS_2 on exposed SiO_2 is to the left of the arrow. An intentional scratch following MoS_2 growth highlights the contrast between the MoS_2-graphene film and bare SiO_2 (upper right corner, Figure 1b). The MoS_2 forms a continuous layer on the entirety of the substrate, indicating that heterostructure growth could be scaled to larger dimensions.

AFM is utilized to investigate the topography of the as-grown MoS_2/graphene/SiO_2/Si heterostructures. **Figure 2**a displays a 5 μm × 5 μm image of the MoS_2-graphene film, while Figure 2b shows an image of the graphene film alone. The ripples and wrinkles present in large-area graphene (Figure 2b) are also apparent in the MoS_2 grown on graphene, indicating that the

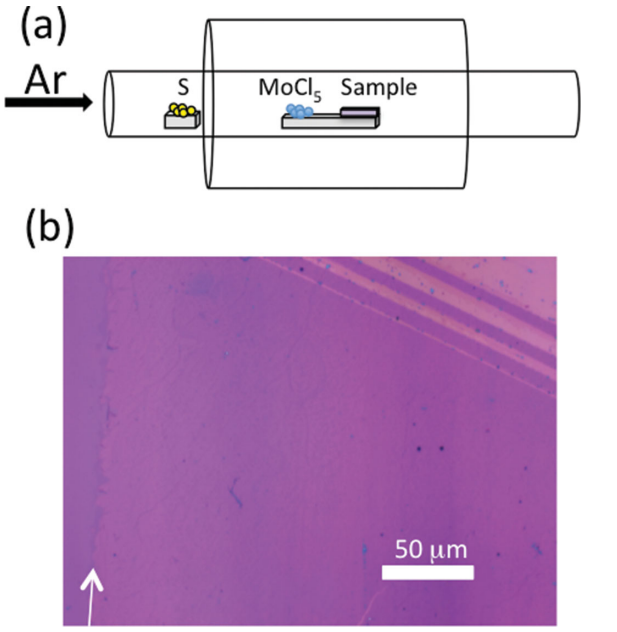

Figure 1. a) Schematic of the furnace set-up for MoS_2 growth on graphene. b) Optical image following the growth procedure. The resulting MoS_2 is continuous and uniform on graphene (to the right of the arrow) as well as on SiO_2 (to the left of the arrow). The heterostructure is intentionally scratched in the upper right corner to indicate contrast with bare SiO_2.

MoS_2 growth process results in a uniform film that follows the contours of the substrate. The height profiles along the surface of MoS_2-graphene (Figure 2c) and bare graphene (Figure 2d) are nearly analogous. We observe small clusters of thicker materials attributed to residues that have not been fully removed during the graphene cleaning procedure, rather than non-uniform MoS_2 growth, as similar clusters are apparent on bare graphene (Figure 2b). Both MoS_2-graphene and bare graphene exhibit an rms roughness less than 0.5 nm. We observe no variations in the number of layers, as confirmed by photoluminescence and

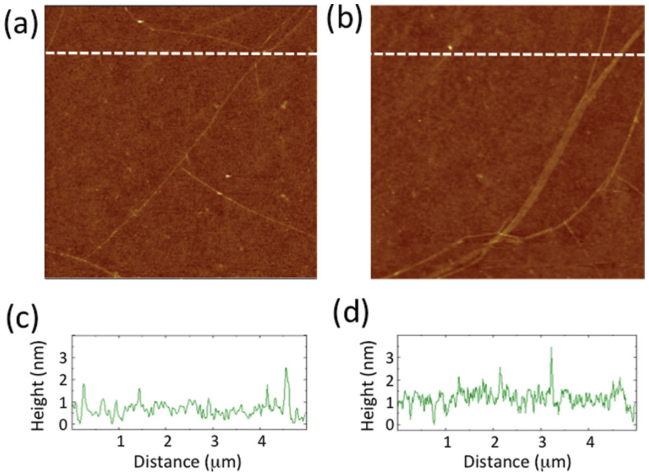

Figure 2. AFM images of a 5 μm × 5 μm area. a) The image of the MoS_2-graphene heterostructure and b) graphene substrate for comparison. c,d) Height profiles along the dotted line in (a) and (b), respectively. The rms roughness is below 0.5 nm before and after MoS_2 growth.

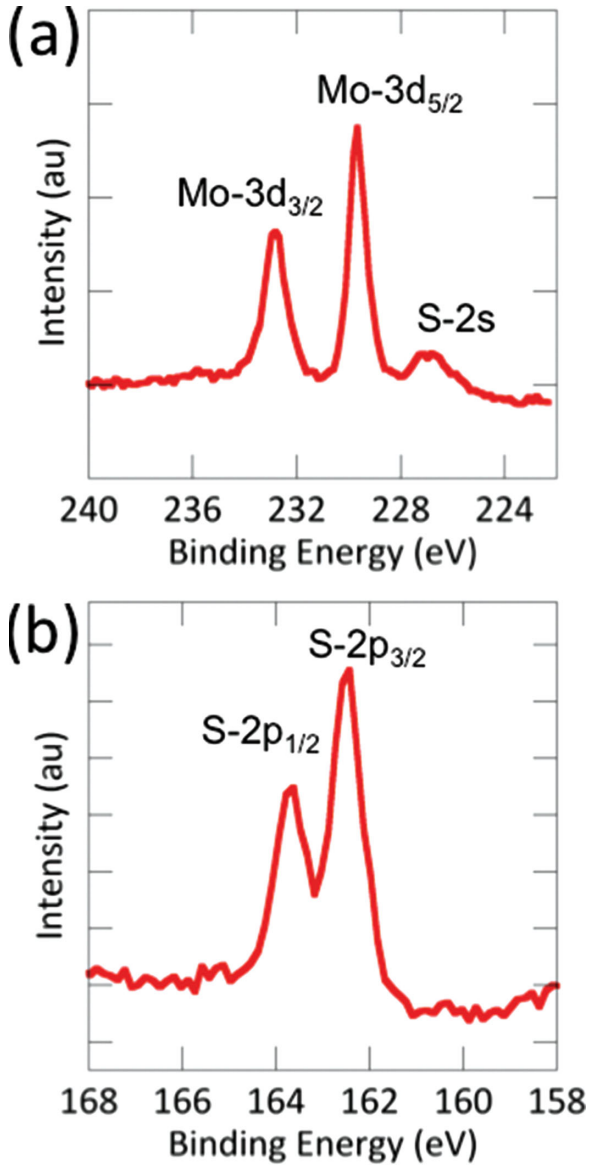

Figure 3. Core binding energies determined using XPS spectra. a) Mo 3d peaks are present at 232.6 eV and 229.5 eV, with S 2s at 226 eV. b) S peaks are present at 163.5 eV and 162.2 eV. XPS indicate stoichiometric MoS_2 synthesis on graphene.

Raman spectroscopy (discussed below), nor any indication that ripples or edges of graphene serve as nucleation sites for the MoS_2 growth.

X-ray photoelectron spectroscopy is used to probe the chemical composition of the as-grown films (which are exposed to atmosphere before loading into the XPS system). Spectra are obtained with monochromated Al Ka radiation using a 400 µm aperture. **Figure 3**a displays Mo 3d peaks at 232.6 eV and 229.5 eV, corresponding to the $3d_{5/2}$ and $3d_{3/2}$ doublet, as well as the sulfur 2s peak at 226 eV. The peaks at 163.5 eV and 162.2 eV (Figure 3b) correspond to the S $p_{1/2}$ and S $p_{3/2}$ orbital. The observed binding energies are consistent with previously reported values for MoS_2[29,35] and confirm the expected charge states of S^{2-} and Mo^{4+} in the MoS_2. The Mo 3d peaks show no

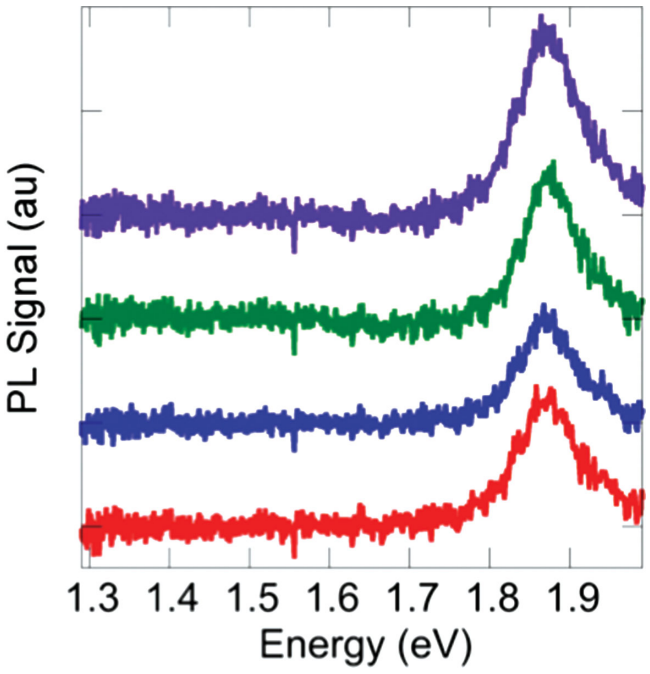

Figure 4. Photoluminescence spectra from the heterostructure samples. The four displayed spectra (offset for clarity) span a 2 mm distance and are representative of the 2.5 mm × 2.5 mm area investigated. The single emission peak at 1.88 eV and absence of lower emission peaks confirms atomically thin MoS_2 grown on graphene.

indication of additional peaks at lower binding energy (indicative of metallic Mo) or at higher binding energy (indicative of MoO_2 or MoO_3) attesting to the quality of the growth. Furthermore, XPS spectra measure an S:Mo ratio of 2, confirming stoichiometric MoS_2 synthesis on graphene. Instrumentation limitations and fitting procedures lead to a conservative error of less than 5% in the stoichiometry value.

The MoS_2 on graphene samples are further investigated with photoluminescence spectroscopy measurements. PL is a useful technique for readily distinguishing single and multilayer MoS_2. The PL emission of monolayer MoS_2 at room temperature is characterized by a single peak, typically between 1.82 and 1.89 eV. The exact energy is sample dependent and is influenced by both the environment[36] and the synthesis method.[28,29] Emission from two or more layers of MoS_2 shifts the peak to lower energy, and the intensity is reduced significantly. For multiple layers, the indirect gap transition starts to develop around 1.3 eV.[12,13] PL spectra are measured at room temperature over a 2.5 mm × 2.5 mm area at discrete steps of 0.5 mm. **Figure 4** displays four consecutive measurements, offset for clarity, spanning a lateral distance of 2 mm. All spectra exhibit a strong single-energy emission peak at 1.88 eV with no indication of lower energy peaks and linewidth of ≈120 meV. This is consistent with monolayer MoS_2 grown with CVD and further confirms the uniformity of the films.

Raman spectroscopy is a useful tool to investigate properties of the graphene underlayer in addition to MoS_2. The two characteristic peaks in MoS_2 are the E^1_{2g} and A_{1g} modes, corresponding to the in-plane and out-of-plane vibrations of the Mo-S bond, respectively. Bulk MoS_2 material exhibits peaks at ≈382 cm^{-1} and

≈407 cm^{-1} with a peak separation (Δk) of 25 cm^{-1}.[37] As MoS_2 films approach monolayer thickness, Δk is found to decrease, and the separation between peaks can be used to identify the number of MoS_2 layers. Experimentally measured Δk for monolayer MoS_2 on an SiO_2 substrate are typically in the range of 18–20 cm^{-1}, with bilayer increasing to ≈22 cm^{-1}, and trilayer to ≈23 cm^{-1}.[30,37,38]

Raman spectra are measured at room temperature using a 488 nm laser with a spot size ≈0.4 μm and power below 1 mW. A typical Raman spectrum is displayed as the upper trace in **Figure 5**a, and exhibits a Δk of 21.3 cm^{-1}. MoS_2 grown concurrently on bare SiO_2 witness substrate exhibits $\Delta k \approx 20$ cm^{-1} as shown in the lower trace, typical of single layer MoS_2 on an SiO_2 substrate. The larger peak separation observed in our heterostructure samples is a consequence of the graphene substrate, and has been observed in other experimental works investigating exfoliated MoS_2-graphene samples.[39,40] The peak separation of ≈21 cm^{-1} observed for our CVD-synthesized MoS_2-graphene heterostructures is thus indicative of monolayer MoS_2 growth, as corroborated by the PL measurements discussed above.

To examine the uniformity across the heterostructure sample on the typical device scale, spectra are acquired at 0.5 μm spacing across a 10 μm × 10 μm area (Figure 5b). The positions of both E^1_{2g} and A_{1g} are constant across the sample surface, with variation in the peak separation ≤ 0.5 cm^{-1}. Furthermore, the uniformity persists over much larger areas, as can be seen in the 3 mm × 3 mm area displayed in Figure 5c.

Raman also provides information on how the overgrowth of MoS_2 impacts the underlying graphene. The graphene peaks of interest are the G, 2D and D peaks as labeled in Figure 5d, with the D peak indicating the presence of defects such as edge states or vacancies. Prior to MoS_2 growth, we observe all three peaks (black line in Figure 5d), with a very low D peak intensity. Peak positions and the Gaussian lineshape of the 2D peak confirm monolayer graphene.[41] Following the MoS_2 growth (red line in Figure 5d) a small increase in the D/G ratio is observed as well as a shift towards higher wavenumber for both 2D and G peaks. The MoS_2 film synthesis on top slightly attenuates the Raman signal, resulting in a lower signal to noise ratio in the graphene spectra. Control samples have ruled out elevated temperature as the source of defects, indicating the interaction with the chemical precursors results in defect formation, either as vacancies or sp^3 bonding. Sulfur has been shown to interact with graphene at elevated temperatures,[42] and is the likely source of the enhanced D peak following MoS_2 growth.

Raman spectroscopy can also indicate charge doping, strain, or a modification of graphene's electronic band structure due to van der Waals forces which we refer to as interlayer coupling. A modulation of electronic band structure near the Dirac point modifies the Fermi velocity, v_F, of graphene and is apparent in the Raman spectra. Both charge doping and strain produce shifts in the 2D as well as the G peak position, and the degree to which the peaks are shifted is distinct for each effect. In contrast, interlayer coupling modifies only the 2D peak position, allowing this effect to be distinguished from strain and doping. Despite being weak in layered materials, the van der Waals interaction is capable of modifying graphene's electronic band structure in graphene-hBN heterostructures,[43] and motivates investigation of interlayer coupling in our MoS_2-graphene heterostructures.

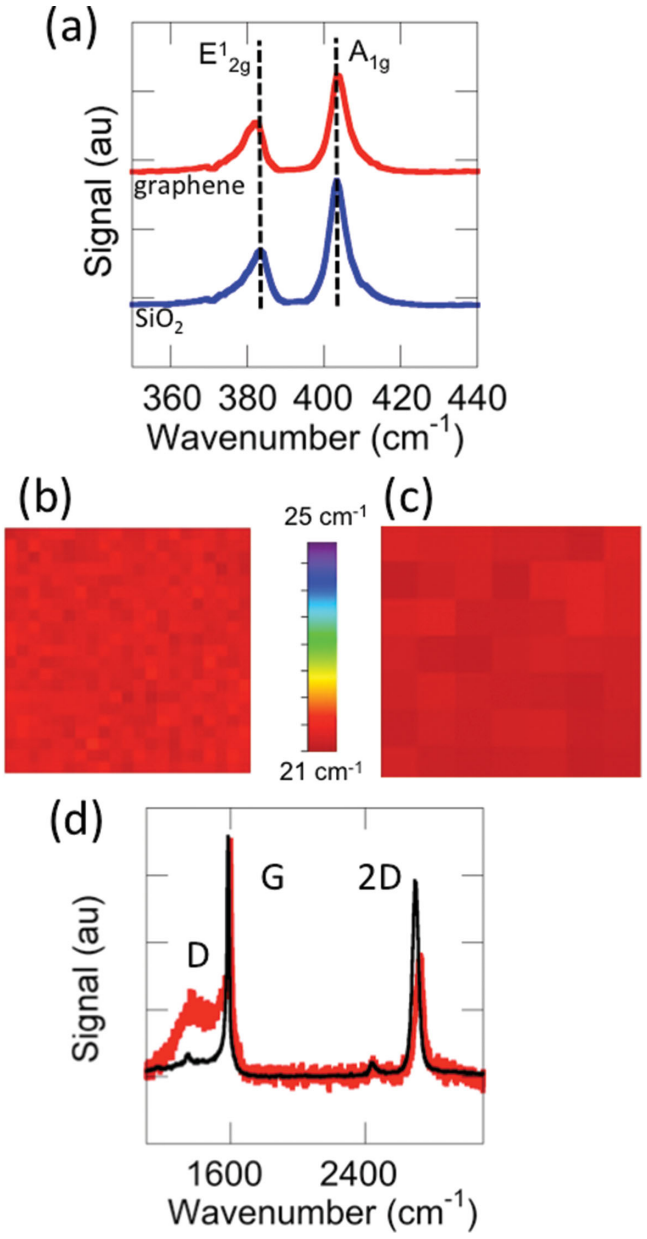

Figure 5. Raman spectroscopy of heterostructure samples. a) Comparison of Raman peaks for MoS_2 synthesized on graphene (upper, red) and on SiO_2 (lower, blue). The characteristic MoS_2 E^1_{2g}, and A_{1g} peaks are identified. The peak separation is 21.3 cm^{-1}, consistent with single layer MoS_2 on graphene. b,c) Raman maps displaying the peak separation measured across a 10 μm ×10 μm area and a 3 mm × 3 mm area, respectively, confirming single monolayer MoS_2 growth. d) Spectra of graphene peaks before (black line) and after (red line) CVD of MoS_2.

Following an analysis procedure outlined in refs [43,44], we plot the 2D vs G peak position of spectra obtained from bare graphene and MoS_2-graphene heterostructures (blue circles) in **Figure 6**. Bare graphene shows variations due to deviations in strain across the surface, as expected. Referring to Figure 6, if the presence of MoS_2 leads to compressive strain in graphene, a shift along the direction of the black vector labeled Δ_s is expected for the MoS_2-graphene Raman spectra. Charge doping

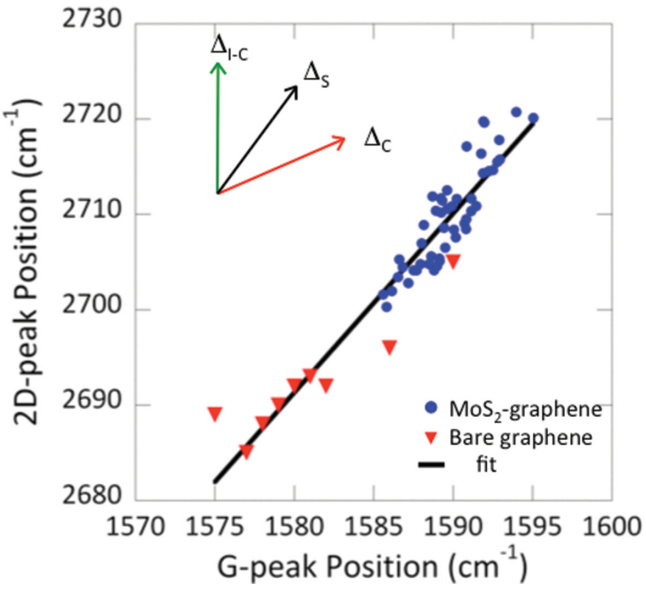

Figure 6. Analysis of Raman spectra for bare graphene and MoS_2-graphene heterostructures. The position of the graphene 2D peak is plotted versus the position of the graphene G peak. Shifts along the arrows labeled $\Delta_{i\text{-}c}$, Δ_s, and Δ_c indicate the presence of interlayer coupling, compressive strain, and hole doping, respectively. The trend observed for MoS_2-graphene indicates compressive strain in the graphene following MoS_2 synthesis.

has a smaller affect on the shift in 2D position, and the addition of holes will produce shifts along the red vector labeled Δ_c in Figure 6. Interlayer coupling affects only the 2D peak position, resulting in a vertical shift along the green vector labeled $\Delta_{i\text{-}c}$ in Figure 6. As evident in Figure 6, data for both bare graphene and MoS_2-graphene heterostructures are well fit by a line with a slope of 1.9 along the black vector Δ_s. The observed behavior suggests compressive strain is the dominant factor in both bare graphene-SiO_2 and MoS_2-graphene-SiO_2 heterostructures, with the effect being more pronounced with the MoS_2 overlayer. The additional compressive strain in MoS_2-graphene films may be a result of the different coefficients of thermal expansion exhibited in graphene and MoS_2. The MoS_2 film may expand more than graphene at the elevated synthesis temperature and gradually compresses the graphene film as the heterostructure cools to room temperature. From this analysis there is no indication that the synthesized MoS_2 modifies the electronic band structure of graphene.

3. Conclusion

In conclusion, we have demonstrated synthesis of large-area heterostructures composed of MoS_2 on graphene. The samples are investigated with optical microscopy, AFM, XPS, PL and Raman spectroscopy and are uniform, continuous, and atomically thin. The ability to produce large-area 2D heterostructures by direct CVD growth of MoS_2 on graphene provides a new avenue as opposed to the commonly used (and tedious) method of multiple mechanical exfoliations. The availability of large scale MoS_2-graphene heterostructures will stimulate investigations into photonic, electronic, and spintronic properties of this new structure and will be a benefit to the scientific community.

Acknowledgements

This work was supported by programs at core programs at the Naval Research Laboratory (NRL). This research was performed while K.M.M held a National Research Council Research Associateship Award at NRL. The authors acknowledge use of facilities in the NRL Nanoscience Institute and thank David Zapotok and Dean St. Amand for technical support. K.M.M. synthesized the MoS_2– graphene samples; J.T.R. provided CVD graphene substrates; K.M.M., A.T.H., and J.C.C., and G.G.J. performed optical and chemical analysis. K.M.M. and B.T.J. wrote the manuscript. All authors contributed to the interpretation of the data and editing of the manuscript.

Received: May 9, 2014
Revised: July 1, 2014
Published online: August 21, 2014

[1] A. K. Geim, K. S. Novoselov, *Nat. Mater.* **2007**, *6*, 183.
[2] K. S. Kim, Y. Zhao, H. Jang, S. Y. Lee, J. M. Kim, K. S. Kim, J.-H. Ahn, P. Kim, J.-Y. Choi, B. H. Hong, *Nature* **2009**, *457*, 706.
[3] V. Tozzini, V. Pellegrini, *Phys. Chem. Chem. Phys.* **2013**, *15*, 80.
[4] J. T. Robinson, F. K. Perkins, E. S. Snow, Z. Wei, P. E. Sheehan, *Nano Lett.* **2008**, *8*, 3137.
[5] F. Schedin, A. K. Geim, S. V. Morozov, E. W. Hill, P. Blake, M. I. Katsnelson, K. S. Novoselov, *Nat. Mater.* **2007**, *6*, 652.
[6] G.-H. Lee, Y.-J. Yu, X. Cui, N. Petrone, C.-H. Lee, M. S. Choi, D.-Y. Lee, C. Lee, W. J. Yoo, K. Watanabe, T. Taniguchi, C. Nuckolls, P. Kim, J. Hone, *ACS Nano* **2013**, *7*, 7931.
[7] R. K. Singh Raman, P. Chakraborty Banerjee, D. E. Lobo, H. Gullapalli, M. Sumandasa, A. Kumar, L. Choudhary, R. Tkacz, P. M. Ajayan, M. Majumder, *Carbon* **2012**, *50*, 4040.
[8] Q. H. Wang, K. Kalantar-Zadeh, A. Kis, J. N. Coleman, M. S. Strano, *Nat. Nanotechnol.* **2012**, *7*, 699.
[9] S. Das, R. Gulotty, A. V. Sumant, A. Roelofs, *Nano Lett.* **2014**, *14*, 2861.
[10] K. S. Novoselov, D. Jiang, F. Schedin, T. J. Booth, V. V. Khotkevich, S. V. Morozov, A. K. Geim, *Proc. Natl. Acad. Sci. U.S.A.* **2005**, *102*, 10451.
[11] J. N. Coleman, M. Lotya, A. O'Neill, S. D. Bergin, P. J. King, U. Khan, K. Young, A. Gaucher, S. De, R. J. Smith, I. V. Shvets, S. K. Arora, G. Stanton, H.-Y. Kim, K. Lee, G. T. Kim, G. S. Duesberg, T. Hallam, J. J. Boland, J. J. Wang, J. F. Donegan, J. C. Grunlan, G. Moriarty, A. Shmeliov, R. J. Nicholls, J. M. Perkins, E. M. Grieveson, K. Theuwissen, D. W. McComb, P. D. Nellist, V. Nicolosi, *Science* **2011**, *331*, 568.
[12] K. F. Mak, C. Lee, J. Hone, J. Shan, T. F. Heinz, *Phys. Rev. Lett.* **2010**, *105*, 136805.
[13] A. Splendiani, L. Sun, Y. Zhang, T. Li, J. Kim, C.-Y. Chim, G. Galli, F. Wang, *Nano Lett.* **2010**, *10*, 1271.
[14] C. H. Lui, K. F. Mak, J. Shan, T. F. Heinz, *Phys. Rev. Lett.* **2010**, *105*, 127404.
[15] B. Radisavljevic, A. Radenovic, J. Brivio, V. Giacometti, A. Kis, *Nat Nano* **2011**, *6*, 147.
[16] F. K. Perkins, A. L. Friedman, E. Cobas, P. M. Campbell, G. G. Jernigan, B. T. Jonker, *Nano Lett.* **2013**, *13*, 668.
[17] S. Balendhran, S. Walia, H. Nili, J. Z. Ou, S. Zhuiykov, R. B. Kaner, S. Sriram, M. Bhaskaran, K. Kalantar-zadeh, *Adv. Funct. Mater.* **2013**, *23*, 3952.
[18] D. Jariwala, V. K. Sangwan, L. J. Lauhon, T. J. Marks, M. C. Hersam, *ACS Nano* **2014**, *8*, 1102.

[19] R. Ganatra, Q. Zhang, *ACS Nano* **2014**, 8, 4074.
[20] S. Z. Butler, S. M. Hollen, L. Cao, Y. Cui, J. A. Gupta, H. R. Gutiérrez, T. F. Heinz, S. S. Hong, J. Huang, A. F. Ismach, E. Johnston-Halperin, M. Kuno, V. V. Plashnitsa, R. D. Robinson, R. S. Ruoff, S. Salahuddin, J. Shan, L. Shi, M. G. Spencer, M. Terrones, W. Windl, J. E. Goldberger, *ACS Nano* **2013**, *7*, 2898.
[21] A. K. Geim, I. V. Grigorieva, *Nature* **2013**, *499*, 419.
[22] L. Britnell, R. V. Gorbachev, R. Jalil, B. D. Belle, F. Schedin, A. Mishchenko, T. Georgiou, M. I. Katsnelson, L. Eaves, S. V. Morozov, N. M. R. Peres, J. Leist, A. K. Geim, K. S. Novoselov, L. A. Ponomarenko, *Science* **2012**, *335*, 947.
[23] K. Roy, M. Padmanabhan, S. Goswami, T. P. Sai, G. Ramalingam, S. Raghavan, A. Ghosh, *Nat. Nanotechnol.* **2013**, *8*, 826.
[24] S. Bertolazzi, D. Krasnozhon, A. Kis, *ACS Nano* **2013**, *7*, 3246.
[25] X. Li, W. Cai, J. An, S. Kim, J. Nah, D. Yang, R. Piner, A. Velamakanni, I. Jung, E. Tutuc, S. K. Banerjee, L. Colombo, R. S. Ruoff, *Science* **2009**, *324*, 1312.
[26] A. Reina, X. Jia, J. Ho, D. Nezich, H. Son, V. Bulovic, M. S. Dresselhaus, J. Kong, *Nano Lett.* **2008**, *9*, 30.
[27] T. Kobayashi, M. Bando, N. Kimura, K. Shimizu, K. Kadono, N. Umezu, K. Miyahara, S. Hayazaki, S. Nagai, Y. Mizuguchi, Y. Murakami, D. Hobara, *Appl. Phys. Lett.* **2013**, *102*.
[28] Y. Yu, C. Li, Y. Liu, L. Su, Y. Zhang, L. Cao, *Sci. Rep.* **2013**, *3*.
[29] J. Mann, D. Sun, Q. Ma, J.-R. Chen, E. Preciado, T. Ohta, B. Diaconescu, K. Yamaguchi, T. Tran, M. Wurch, K. Magnone, T. F. Heinz, G. L. Kellogg, R. Kawakami, L. Bartels, *Eur. Phys. J. B* **2013**, *86*, 1.
[30] S. Najmaei, Z. Liu, W. Zhou, X. Zou, G. Shi, S. Lei, B. I. Yakobson, J.-C. Idrobo, P. M. Ajayan, J. Lou, *Nat Mater* **2013**, *12*, 754.
[31] Y. Li, H. Wang, L. Xie, Y. Liang, G. Hong, H. Dai, *J. Am. Chem. Soc.* **2011**, *133*, 7296.
[32] Y. Shi, W. Zhou, A.-Y. Lu, W. Fang, Y.-H. Lee, A. L. Hsu, S. M. Kim, K. K. Kim, H. Y. Yang, L.-J. Li, J.-C. Idrobo, J. Kong, *Nano Lett.* **2012**, *12*, 2784.
[33] Y.-C. Lin, N. Lu, N. Perea-Lopez, J. Li, Z. Lin, X. Peng, C. H. Lee, C. Sun, L. Calderin, P. N. Browning, M. S. Bresnehan, M. J. Kim, T. S. Mayer, M. Terrones, J. A. Robinson, *ACS Nano* **2014**, *8*, 3715.
[34] X. Ling, Y.-H. Lee, Y. Lin, W. Fang, L. Yu, M. S. Dresselhaus, J. Kong, *Nano Lett.* **2014**, *14*, 464.
[35] K.-K. Liu, W. Zhang, Y.-H. Lee, Y.-C. Lin, M.-T. Chang, C.-Y. Su, C.-S. Chang, H. Li, Y. Shi, H. Zhang, C.-S. Lai, L.-J. Li, *Nano Lett.* **2012**, *12*, 1538.
[36] G. Plechinger, F.-X. Schrettenbrunner, J. Eroms, D. Weiss, C. Schüller, T. Korn, *Phys. Status Solidi (RRL)* **2012**, *6*, 126.
[37] C. Lee, H. Yan, L. E. Brus, T. F. Heinz, J. Hone, S. Ryu, *ACS Nano* **2010**, *4*, 2695.
[38] Y. Zhan, Z. Liu, S. Najmaei, P. M. Ajayan, J. Lou, *Small* **2012**, *8*, 966.
[39] M. Buscema, G. Steele, H. J. Zant, A. Castellanos-Gomez, *Nano Res.* **2014**, *7*, 1.
[40] W. Zhang, C.-P. Chuu, J.-K. Huang, C.-H. Chen, M.-L. Tsai, Y.-H. Chang, C.-T. Liang, Y.-Z. Chen, Y.-L. Chueh, J.-H. He, M.-Y. Chou, L.-J. Li, *Sci. Rep.* **2014**, *4*.
[41] A. C. Ferrari, J. C. Meyer, V. Scardaci, C. Casiraghi, M. Lazzeri, F. Mauri, S. Piscanec, D. Jiang, K. S. Novoselov, S. Roth, A. K. Geim, *Phys. Rev. Lett.* **2006**, *97*, 187401.
[42] H. L. Poh, P. Šimek, Z. Sofer, M. Pumera, *ACS Nano* **2013**, *7*, 5262.
[43] G. Ahn, H. R. Kim, T. Y. Ko, K. Choi, K. Watanabe, T. Taniguchi, B. H. Hong, S. Ryu, *ACS Nano* **2013**, *7*, 1533.
[44] J. E. Lee, G. Ahn, J. Shim, Y. S. Lee, S. Ryu, *Nat Commun* **2012**, *3*, 1024.